Photon-emission spectra of the H_2^+ molecular ion in an intense laser field

T. Zuo, S. Chelkowski, and A. D. Bandrauk
Laboratoire de Chimie Théorique, Faculté des Sciences, Université de Sherbrooke, Sherbrooke, Québec, Canada J1K 2R1
(Received 10 November 1993)

Photon-emission spectra of the H_2^+ molecular ion in an intense, linearly polarized laser field (wavelength $\lambda = 1064$ nm and intensities $10^{13} \leq I \leq 10^{14}$ W/cm^2) have been calculated using an exact method and compared to two-level models. The exact calculation requires solving a three-dimensional time-dependent Schrödinger equation which allows a full treatment of all the electronic states of H_2^+ as a function of the internuclear separation R. Three separate excitation regions can be defined which are associated with the $1\sigma_g$-$1\sigma_u$ charge-resonant (CR) transition of the H_2^+ molecular ion: (1) for small R, the multiphoton excitation region; (2) for intermediate R, the near-resonant excitation region; and (3) for large R, the strong-coupling region. Two- and three-level models are used for the description of these excitations of the CR states. We will show in this work that (a) in the multiphoton excitation region, an approximate solution of the laser-driven CR states is given by WKB solutions of a Mathieu equation; (b) in the near-resonant region, Rabi or Mollow triplets are obtained for all the harmonics; and (c) in the strong-coupling region, an analytic two-level solution for the CR state excitation reproduces well the exact results. The effects of ground-continuum coupling and ionization is shown to be important for laser intensities $I \geq 10^{14}$ W/cm^2.

PACS number(s): 33.80.Rv, 33.90.+h, 42.50.Hz, 42.65.Ky

I. INTRODUCTION

The study of photon-emission spectra of quantum systems in intense laser fields has attracted a great amount of attention in recent years. One of the most prominent features of the photon-emission spectra in very intense laser fields is the emission of light by a quantum system at frequencies which are multiples of the driving laser frequency, otherwise known as harmonic generation (HG). Photon-emission spectra have been studied for many quantum systems from two-level system to single-electron atoms (for a review, see, e.g., Ref. [1]).

It is known that symmetric molecular ions have pairs of charge-resonant (CR) states which are very strongly coupled to electromagnetic fields, especially at large internuclear separation R [2]. Bandrauk and co-workers first pointed out the importance of these CR states as sources of highly nonlinear laser-induced effects in molecules [3]. Ivanov, Corkum, and Dietrich have examined two-level models of symmetric molecular ions for large R where the Rabi frequency is much greater than the transition frequency of the CR states [4]. Recently, Zuo, Chelkowski, and Bandrauk have calculated the HG spectra for the H_2^+ molecular ion in very intense laser fields by solving exactly a three-dimensional (3D) time-dependent Schrödinger equation [5]. The molecular ion is found to be a highly efficient source for HG at larger R due to its CR states when compared with atomic systems. At small R and high intensity ($I \geq 10^{14}$ W/cm^2), the molecular system is found to behave analogously to an atomic system. In this latter case, the laser intensity is high enough that ground-continuum transitions dominate the whole process and the details of bound state structure become less important. As a result the HG spectra show well resolved peaks of odd harmonics usually extending to very high order.

The present work concentrates on the calculation of the photon-emission spectra of the H_2^+ molecular ion for moderately intense laser fields ($\sim 10^{13}$ W/cm^2). As will been seen, at small R, harmonic and nonharmonic peaks coexist. We will show that this is explained by an analytic solution of the equations for the laser-driven CR states: these are obtained by a WKB analysis of the Mathieu equation for the time-dependent Schrödinger equation of a two-level system in a laser field. At intermediate R, we study an interesting case where the transition frequency is close to the laser frequency (near resonant). We show that the well-known Rabi or Mollow triplets are obtained for all the harmonic peaks observable for a given intensity and these are correlated to the quasienergies of a two-level system. At large R, the strong-coupling case, we will show again that each harmonic peak is accompanied by two sidebands which are described by analytic formulas in a two-level approximation. Couplings beyond the two lowest CR states and continuum (ionization) states are shown to become important at intensities above 10^{14} W/cm^2.

Since the numerical techniques of obtaining the 3D time-dependent solutions and calculating the spectra once the solutions are available have been discussed in detail in previous work [5,6], they are not repeated here. Instead, analytic solutions based on WKB-Mathieu functions (which is new to our knowledge) are discussed in detail in order to explain the spectra. Results for the three regions, the multiphoton excitation region, the near resonant region, and the strong coupling region will be presented and discussed in Secs. II, III, and IV, respectively. Conclusions will be drawn in Sec. V.

II. THE MULTIPHOTON EXCITATION REGION

Figure 1 shows some of the lowest electronic levels of the H_2^+ molecular ion [7]. We see that at $R = 2$ a.u. (the equilibrium separation of H_2^+) the ionization potential is 1.1 a.u. and the energy separation between the $1\sigma_g$ state and $1\sigma_u$ state is 0.436 a.u., i.e., starting from the ground state H_2^+ one needs to absorb 25.7 ($\lambda = 1064$ nm) photons to reach the ionization continuum and 10.18 photons to reach the first excited state, $1\sigma_u$. Since our calculations show that very little ionization ($2.3\times10^{-4}\%$) has occurred for H_2^+ interacting with a $\lambda = 1064$ nm, $I = 10^{13}$ W/cm^2, flat laser pulse for 30 cycles (107 fs), we call this region the multiphoton excitation region (the corresponding ionization rate is 6.4×10^8/sec.) [5].

The photon-emission spectra obtained from the full (3D time-dependent) calculation is obtained from the power spectrum [5]

$$|d(\omega)|^2 = \left| \int_{T_1}^{T_2} d(t) e^{-i\omega t} dt/(T_2 - T_1) \right|^2, \qquad (1a)$$

where the field-induced dipole moment $d(t)$ is obtained from the exact wave function $\psi(t)$,

$$d(t) = \langle \psi(t)|z|\psi(t)\rangle. \qquad (1b)$$

In Fig. 2 we see that harmonic peaks appear only up to the third order. Higher-order peaks are immersed into a broad background dominated by a prominent (hereafter referred to as multiphoton resonance) peak at energy $10.18\hbar\omega$. This is the resonance condition for the $1\sigma_g$ to the $1\sigma_u$ transition or CR transition. Careful examination of Fig. 2 indicates that satellites occur at 8.18 and $12.18\hbar\omega$. We will show next that these features can be explained by a two-level analysis. The emitted radiation at $14.6\hbar\omega$, $16.6\hbar\omega$, $18.6\hbar\omega$, etc. comes from higher coupled H_2^+ levels, notably the $1\sigma_g \rightarrow 1\sigma_u \rightarrow 2\sigma_g$ transitions in the laser field as we show below. Figure 3(a) gives the spectra calculated from an exact numerical solution of the time-dependent Schrödinger equation involving only the $1\sigma_g$ and the $1\sigma_u$ states at the same laser intensity.

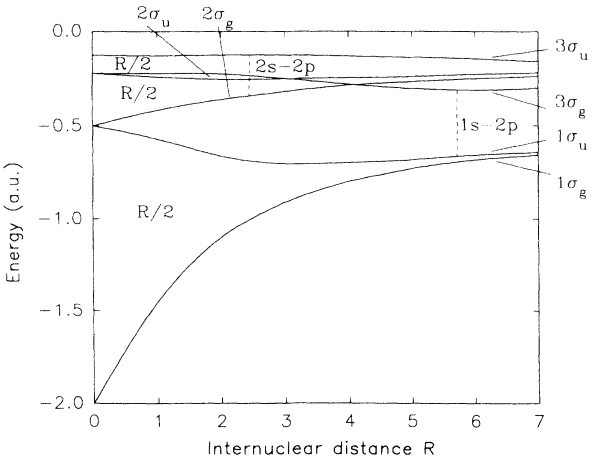

FIG. 1. Energy levels of some lowest states of H_2^+.

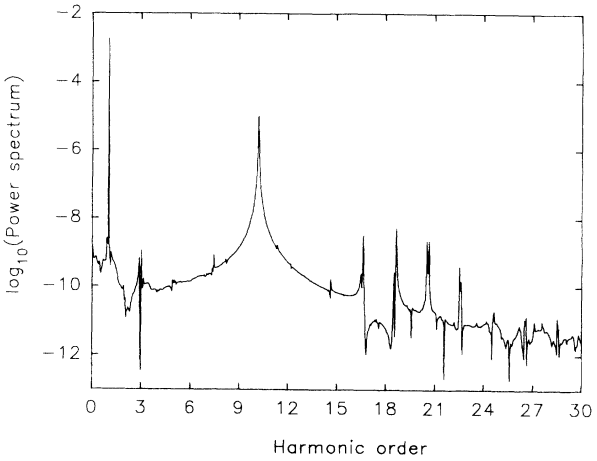

FIG. 2. Photon-emission spectrum of H_2^+ at $R = 2$ a.u., $I = 1 \times 10^{13}$W/cm^2, $\lambda = 1064$ nm. The laser pulse is given by $-E_0 \sin(\omega t)$ for $0 < t < 30$ cycles (106.5 fs).

The fact that both the harmonic peaks and the multiphoton resonance peaks appear clearly in the two-level calculations suggests that further analysis of the two-level system can be useful for the explanation of the harmonic and especially the multiphoton resonance peaks. We perform this analysis through an analytic solution obtained by making appropriate approximations to the two-level time-dependent Schrödinger equation.

For a two-level system, one writes the time-dependent wave function $\psi(t) = c_1(t)\psi_1 + c_2(t)\psi_2$, where ψ_1 and

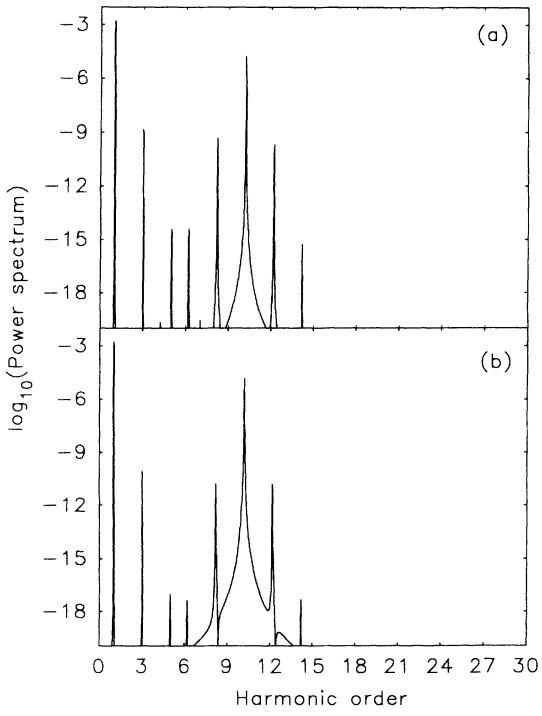

FIG. 3. Same as Fig. 2 but with two-level calculation. (a) exact time-dependent calculation; (b) WKB-Mathieu calculation.

ψ_2 are the time-independent eigenfunctions of levels 1 and 2. The time-dependent Schrödinger equation for this two-level system interacting with a laser field becomes

$$i\dot{c_1} = -\omega_0 c_1 + \Omega_R \cos(\omega t) c_2, \tag{2a}$$
$$i\dot{c_2} = \Omega_R \cos(\omega t) c_1. \tag{2b}$$

Here ω is the laser frequency, ω_0 is the transition frequency ($\hbar\omega_0 = E_2 - E_1$) and $\Omega_R = d_0 E_0$ is the Rabi frequency with d_0 and E_0 being the transition dipole moment between levels 1 and 2 and the maximum absolute amplitude of the external electric field, respectively. Differentiating (2a) one more time one obtains

$$i\ddot{c_1} = -\omega_0 \dot{c_1} + \Omega_R \cos(\omega t)\dot{c_2} - \Omega_R \omega \sin(\omega t) c_2. \tag{3}$$

For nonresonant field excitation, such that $\omega_0 \gg \omega$, the term $\Omega_R \omega \sin(\omega t) c_2$ on the right hand side of (3) is small compared with the other two terms. Consequently by neglecting this term, one obtains by also using (2b) that

$$\ddot{c_1} - i\omega_0 \dot{c_1} + \Omega_R^2 \cos^2(\omega t) c_1 = 0. \tag{4}$$

Making a further approximation that $-i\omega_0 \dot{c_1} = \omega_0^2 c_1$ [in Eq. (2a) this assumes $\omega_0 \gg \Omega_R$], one arrives at the second order equation

$$\ddot{c_1} + [\beta^2 - q\cos(2\underline{t})] c_1 = 0, \tag{5}$$

where $\beta = [(\omega_0^2 + \Omega_R^2/2)/\omega^2]^{1/2}$, $q = (\Omega_R^2/2)/\omega^2$, and $\underline{t} = \omega t - \pi/2$. Equation (5) belongs to the family of the well-known Mathieu equation.

Since it is assumed that $\omega_0 \gg \Omega_R$, then $\beta^2 \gg q$. Under these circumstances, seeking a WKB solution of the type $\exp(\pm i \int p\, \mathrm{d}\underline{t})$ where $p = \sqrt{\beta^2 - q\cos(2\underline{t})} \approx \beta[1 - q/(2\beta^2)\cos(2\underline{t})]$ to (5) is appropriate since the square root has no zeros or turning points. After some manipulation one can show that the normalized WKB solution of (5) satisfying the initial conditions for $\underline{t} = 0$: $c_1 = 1$, $c_2 = 0$ and $\dot{c_1} = i\omega_0$, is given by

$$c_1 = \cos\left[\beta\left(\underline{t} - \frac{q}{4\beta^2}\sin(2\underline{t})\right)\right] + ib\sin\left[\beta\left(\underline{t} - \frac{q}{4\beta^2}\sin(2\underline{t})\right)\right] = A + iB, \tag{6}$$

where $b = \omega_0/[\omega\beta(1 - q/2\beta^2)]$. From trigonometric relations for $\cos(z\sin(\theta))$ and $\sin(z\sin(\theta))$ in terms of Bessel functions $J_n(z)$ [8] we can write that

$$A = \cos[\beta\underline{t} - h\sin(2\underline{t})] \tag{7a}$$
$$= \cos(\beta\underline{t})\sum_{n=0}^{\infty}\epsilon_{2n} J_{2n}(h)\cos(4n\underline{t}) + \sin(\beta\underline{t})\sum_{n=0}^{\infty}\epsilon_{2n+1} \times J_{2n+1}(h)\sin(4n+2)\underline{t}, \tag{7b}$$

$$B = b\sin[\beta\underline{t} - h\sin(2\underline{t})] \tag{7c}$$
$$= b\sin(\beta\underline{t})\sum_{n=0}^{\infty}\epsilon_{2n} J_{2n}(h)\cos(4n\underline{t}) - b\cos(\beta\underline{t})\sum_{n=0}^{\infty}\epsilon_{2n+1} \times J_{2n+1}(h)\sin(4n+2)\underline{t}, \tag{7d}$$

where $\epsilon_0 = 1$; $\epsilon_n = 2, n = 1, \ldots, \infty$, $h = q/(4\beta)$. Using Eq. (2b) and keeping in mind the initial condition that $c_2 = 0$ when $\underline{t} = 0$, we have, furthermore,

$$c_2 = \frac{i\Omega_R}{\omega}\int (A + iB)\sin\underline{t}\,\mathrm{d}\underline{t} + i\frac{\Omega_R}{\omega}B_0$$
$$= -\frac{\Omega_R}{\omega}\int B\sin\underline{t}\,\mathrm{d}\underline{t} + i\frac{\Omega_R}{\omega}\left(\int A\sin\underline{t}\,\mathrm{d}\underline{t} + B_0\right). \tag{8}$$

Here, B_0 is an integration constant which takes a real value so that the initial condition for c_2 is satisfied. The laser induced dipole moment is by definition

$$d(t) = d_0(c_1 c_2^*) + \text{c.c.}$$
$$= \frac{2\Omega_R d_0}{\omega}\left(-A\int B\sin\underline{t}\,\mathrm{d}\underline{t} + B\int A\sin\underline{t}\,\mathrm{d}\underline{t} + B_0 B\right)$$
$$= d_h + d_m, \tag{9}$$

where we have used Eqs. (6) and (8). In Eq. (9), $d_h = \frac{2\Omega_R d_0}{\omega}(-A\int B\sin\underline{t}\,\mathrm{d}\underline{t} + B\int A\sin\underline{t}\,\mathrm{d}\underline{t})$ and $d_m = \frac{2\Omega_R d_0}{\omega}B_0 B$. Using the expansions (7b) and (7d) we obtain readily for each term in (8),

$$\int B\sin\underline{t}\,\mathrm{d}\underline{t} = \frac{b}{4}\sum_{n=0}^{\infty}\epsilon_{2n}J_{2n}(h)\left(\frac{\sin(1-\beta-4n)\underline{t}}{1-\beta-4n} - \frac{\sin(1+\beta+4n)\underline{t}}{1+\beta+4n} + \frac{\sin(1-\beta+4n)\underline{t}}{1-\beta+4n} - \frac{\sin(1+\beta-4n)\underline{t}}{1+\beta-4n}\right)$$
$$-\frac{b}{4}\sum_{n=0}^{\infty}\epsilon_{2n+1}J_{2n+1}(h)\left(\frac{\sin(-1-\beta-4n)\underline{t}}{-1-\beta-4n} - \frac{\sin(3+\beta+4n)\underline{t}}{3+\beta+4n}\right.$$
$$\left.+\frac{\sin(-1+\beta-4n)\underline{t}}{-1+\beta-4n} - \frac{\sin(3-\beta+4n)\underline{t}}{3-\beta+4n}\right), \tag{10a}$$

$$\int A\sin\underline{t}\,\mathrm{d}\underline{t} = \frac{1}{4}\sum_{n=0}^{\infty}\epsilon_{2n}J_{2n}(h)\left(\frac{-\cos(1+\beta+4n)\underline{t}}{1+\beta+4n} + \frac{-\cos(1-\beta-4n)\underline{t}}{1-\beta-4n}\right.$$
$$\left.+\frac{-\cos(1+\beta-4n)\underline{t}}{1+\beta-4n} + \frac{-\cos(1-\beta+4n)\underline{t}}{1-\beta+4n}\right)$$

$$+\frac{1}{4}\sum_{n=0}^{\infty}\epsilon_{2n+1}J_{2n+1}(h)\left(\frac{-\cos(-1+\beta-4n)\underline{t}}{-1+\beta-4n}+\frac{-\cos(3-\beta+4n)\underline{t}}{3-\beta+4n}\right.$$

$$\left.-\frac{-\cos(-1-\beta-4n)\underline{t}}{-1-\beta-4n}-\frac{-\cos(3+\beta+4n)\underline{t}}{3+\beta+4n}\right), \tag{10b}$$

$$B_0=\frac{1}{4}\sum_{n=0}^{\infty}\epsilon_{2n}J_{2n}(h)\left(\frac{1}{1+4n+\beta}+\frac{1}{1-4n-\beta}+\frac{1}{1+4n-\beta}+\frac{1}{1-4n+\beta}\right)$$

$$+\frac{1}{4}\sum_{n=0}^{\infty}\epsilon_{2n+1}J_{2n+1}(h)\left(\frac{1}{-1-4n+\beta}+\frac{1}{3+4n-\beta}-\frac{1}{3+4n+\beta}-\frac{1}{-1-4n-\beta}\right). \tag{10c}$$

We obtain finally from (7a), (7c), (10a), and (10b)

$$d_{\mathrm{h}}=\frac{2\Omega_R d_0}{\omega}\left(-A\int B\sin\underline{t}\,\mathrm{d}\underline{t}+B\int A\sin\underline{t}\,\mathrm{d}\underline{t}\right)=\frac{2\Omega_R d_0}{\omega}$$

$$\times\left[\frac{b}{4}\sum_{n=0}^{\infty}\epsilon_{2n}J_{2n}(h)\left(-\frac{\sin[(1-4n)\underline{t}-h\sin 2\underline{t}]}{1-\beta-4n}+\frac{\sin[(1+4n)\underline{t}+h\sin 2\underline{t}]}{1+\beta+4n}\right.\right.$$

$$\left.-\frac{\sin[(1+4n)\underline{t}-h\sin 2\underline{t}]}{1-\beta+4n}+\frac{\sin[(1-4n)\underline{t}+h\sin 2\underline{t}]}{1+\beta-4n}\right)$$

$$+\frac{b}{4}\sum_{n=0}^{\infty}\epsilon_{2n+1}J_{2n+1}(h)\left(\frac{\sin[(-1-4n)\underline{t}+h\sin 2\underline{t}]}{-1+\beta-4n}-\frac{\sin[(3+4n)\underline{t}-h\sin 2\underline{t}]}{3-\beta+4n}\right.$$

$$\left.\left.+\frac{\sin[(-3-4n)\underline{t}-h\sin 2\underline{t}]}{3+\beta+4n}+\frac{\sin[(-1-4n)\underline{t}-h\sin 2\underline{t}]}{-1-\beta-4n}\right)\right]. \tag{11}$$

Using an expansion like (7d), e.g.,

$$\sin[(1-4n)\underline{t}-h\sin(2\underline{t})]=\sin[(1-4n)\underline{t}]\sum_{n'=0}^{\infty}\epsilon_{2n'}J_{2n'}(h)\cos(4n'\underline{t})-\cos[(1-4n)\underline{t}]\sum_{n'=0}^{\infty}\epsilon_{2n'+1}J_{2n'+1}(h)\sin[(4n'+2)\underline{t}]$$

$$=\frac{1}{2}\sum_{n'=0}^{\infty}\epsilon_{2n'}J_{2n'}(h)\left(\sin\{[1+4(n'-n)]\underline{t}\}+\sin\{[1-4(n+n')]\underline{t}\}\right)$$

$$-\frac{1}{2}\sum_{n'=0}^{\infty}\epsilon_{2n'+1}J_{2n'+1}(h)\left(\sin\{[3+4(n'-n)]\underline{t}+\sin\{[1+4(n+n")]\underline{t}\}\right)$$

$$=\frac{-1}{2}\sum_{n'=0}^{\infty}\epsilon_{2n'}J_{2n'}(h)\left(\cos\{[1+4(n'-n)]\omega t\}+\cos\{[1-4(n+n')]\omega t\}\right)$$

$$+\frac{1}{2}\sum_{n'=0}^{\infty}\epsilon_{2n'+1}J_{2n'+1}(h)\left(\cos\{[3+4(n-n')]\omega t+\cos\{[1+4(n'+n)]\omega t\}\right), \tag{12}$$

where the relation $\underline{t}=\omega t-\pi/2$ has been used, it is easy to show from (12) that (11) only contains frequencies at *odd* harmonics, i.e., $1,3,5,\ldots,(2n+1)\omega$. Equation (11), i.e., d_h generates the odd harmonic spectrum. It can also be shown that the strength of the first harmonic peak is proportional to $(\Omega_R J_0^2(h))^2$, that of the third peak proportional to $(\Omega_R J_0(h)J_1(h))^2$, and that of the fifth peak proportional to $(\Omega_R J_1^2(h))^2$ and so on (if $h\approx\Omega_R^2/8\omega\omega_0$ is small). Thus in the weak field limit ($h\ll 1$) the perturbative formula for the laser-induced dipole moment is recovered, i.e., the dipole moment component of nth harmonic is proportional to the nth power of electric field. Furthermore, from (7d) we obtain

$$
\begin{aligned}
d_{\mathrm{m}} &= \frac{2\Omega_R d_0 B_0 B}{\omega} \\
&= \frac{2\Omega_R d_0}{\omega}\left[B_0\frac{b}{2}\sum_{n=0}^{\infty}\epsilon_{2n}J_{2n}(h)\{\sin(\beta+4n)\underline{t}+\sin(\beta-4n)\underline{t}\}\right. \\
&\quad \left.-B_0\frac{b}{2}\sum_{n=0}^{\infty}\epsilon_{2n+1}J_{2n+1}(h)\{\sin(\beta+4n+2)\underline{t}+\sin(-\beta+4n+2)\underline{t}\}\right] \\
&= \frac{\Omega_R d_0 B_0 b}{\omega}\left[\sum_{n=0}^{\infty}\epsilon_{2n}J_{2n}(h)\{\sin[(\beta+4n)\omega t-\beta\pi/2]+\sin[(\beta-4n)\omega t-\beta\pi/2]\}\right. \\
&\quad \left.-\sum_{n=0}^{\infty}\epsilon_{2n+1}J_{2n+1}(h)\{-\sin[(\beta+4n+2)\omega t-\beta\pi/2]+\sin[(\beta-4n-2)\omega t-\beta\pi/2]\}\right]. \qquad (13)
\end{aligned}
$$

Equation (13) contains *nonharmonic* frequencies at β, $\beta\pm2$,..., $\beta\pm2n$ times the driving frequency ω. These are clearly harmonic sidebands of the resonant frequency $\beta\approx\omega_0$. In fact, since $\beta=\sqrt{\frac{\omega_0^2+\Omega_R^2}{\omega^2}}\approx\omega_0$, the central (broadest) multiphoton resonance peak closely corresponds to the level spacings ω_0. The strengths of these multiphoton resonance peaks decrease according to the order of the Bessel function, i.e., the strength of the $\beta\pm2n$ peak is proportional to $|\Omega_R J_{2n}(h)|^2$. Figure 3(b) gives the spectrum calculated from the above analytic solution. A comparison between Figs. 3(b) and 3(a) shows that the analytic solution is capable to predict all the correct emission frequencies. Quantitative agreement is achieved for the strengths of the first order harmonic peak and the zeroth order multiphoton resonance peak. The analytic solution, therefore, agrees well with the spectra from the exact two-level calculation [Figs. 3(a) and 3(b)] so that the origin of the multiphoton resonance peaks are now easily identifiable. The conditions that the Mathieu-WKB solution is valid is that the photon frequency $\omega\ll\omega_0$ and, furthermore, the resonance frequency $\omega_0\gg\Omega_R=d_0E_0$, the Rabi frequency. These conditions are well satisfied, since for H_2^+ at $R=2$ ($d_0\approx1.05$ a.u.), $\lambda=1064$ nm, $I=10^{13}$ W/cm^2, we have $\omega_0=11.86$ eV; $\Omega_R=0.46$ eV, and $\omega=1.16$ eV. Furthermore, it can be shown that the Mathieu-WKB treatment also applies to an equally separated, equally coupled three-level system. The analysis for this three-level system is very similar to the two-level case, which can be found in the Appendix.

Let us now turn to the explanation of the high-order nonharmonic radiation, i.e., radiation at the frequencies $14.6\hbar\omega$, $16.6\hbar\omega$, etc. We will show that this radiation comes from higher coupled H_2^+ level. Figure 4 is a spectrum from an exact three-level time-dependent calculation. The three levels included are the lowest three levels of H_2^+: the $1\sigma_g$, the $1\sigma_u$, and the $2\sigma_g$. The inclusion of the $2\sigma_g$ level is necessary as the energy separation between the $1\sigma_u$ and the $2\sigma_g$ levels, ω_1 is $7.67\hbar\omega$ (for the $1\sigma_g$ and the $2\sigma_g$ levels, ω_0 is $10.18\hbar\omega$) and the dipole moment is 0.81 a.u. (for the $1\sigma_g$ and the $1\sigma_u$ transition this is 1.05 a.u.). Figure 4 shows that the $1\sigma_g\rightarrow1\sigma_u\rightarrow2\sigma_g$ system radiates at (a) the odd harmonic frequencies (ω, 3ω, ...,); (b) the multiphoton resonant frequencies (10.18ω,$(10.18\pm2)\omega$,...,) and (c) the high-order nonharmonic frequencies ($(17.85\pm1)\omega$,$(17.85\pm3)\omega$,...,).

We will show that all these frequencies can be clearly explained in a Floquet (dressed) picture. According to the Floquet theory [9] the time-dependent wave function $\Psi(t)$ can be expanded into a Floquet series:

$$\Psi(t)=\sum_j\exp(-i\epsilon_j t)\Phi_j(t) \qquad (14a)$$

$$=\sum_j\exp(-i\epsilon_j t)\sum_n\psi_n^j\exp(in\omega t)\ , \qquad (14b)$$

where ϵ_j is the jth quasienergy and in Eq. (14b) we have used the fact that $\Phi_j(t)$ is a periodic function with the same period as the laser. We call ψ_n^j the nth Floquet mode of $\Phi_j(t)$. Next we define a time-correlation function

$$P(\tau)=\langle\Psi(t_0)|\Psi(t_0+\tau)\rangle. \qquad (14c)$$

It can be shown by using (14b) and (14c) that the time-correlation function can be expanded by a Fourier series associated with the dressed state energies (the Floquet or quasienergies), i.e.,

$$P(\tau)=\sum_n\sum_j d_n^j\exp[-i(\epsilon_j-n\omega)\tau], \qquad (14d)$$

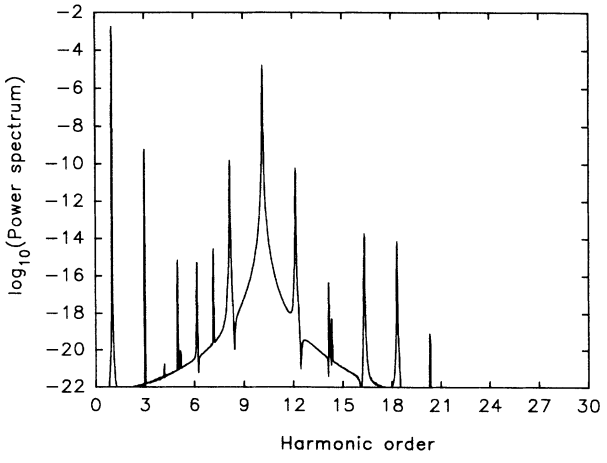

FIG. 4. Same as Fig. 2 but with three-level calculation involving the $1\sigma_g\rightarrow1\sigma_u\rightarrow2\sigma_g$ transitions.

where d_n^j are the corresponding expansion coefficients [10]. The power spectrum of the time-correlation function is given by

$$|P(\omega)|^2 = \left| \int_{T_1}^{T_2} P(\tau) e^{-i\omega\tau} d\tau / (T_2 - T_1) \right|^2 , \qquad (14e)$$

The Floquet energies are then obtained from the power spectrum of the Fourier series. Figure 5 gives the Fourier power spectrum of the time-correlation function of the three-level system described above. It is seen that in Fig. 5 three quasienergies can be readily identified. These are marked as 1–3. Each peak corresponds to a Floquet mode ψ_n^j which has a definite parity $\sigma_j(-1)^n$, where σ_j is the parity of the jth bare state of the system [11]. The transitions between pairs of the Floquet mode with opposite parities (even parity +; odd parity − in Fig. 5) give rise to the radiation at various frequencies as illustrated: (1) the harmonic frequencies indicated by solid horizontal lines; (2) the multiphoton resonant frequencies by dashed horizontal lines; and (3) the high-order nonharmonic frequencies by the dotted horizontal lines. It is noted, however, that the high-order nonharmonic radiation from the full calculation (Fig. 2) is much stronger than that from the three-level calculation. The high-order nonharmonic peaks are also split and slightly shifted from the three-level predictions (e.g., $16.6\hbar\omega$ vs $16.85\hbar\omega$). These are attributed to excitations of even higher H_2^+ levels and continuum, which are included in the full calculation. One sees clearly from the exact calculation (Fig. 2) and the three-level calculation that the $1\sigma_g \rightarrow 1\sigma_u$ transition emits at its resonant frequency $\omega_0 = 10.18\omega$ with even sidebands, $\omega_0 \pm 2\omega$. This is in agreement with the two-level analytic solution, Eq. (13). Higher sidebands occur at the combination frequencies $\omega' = \omega_0 + \omega_1 \pm (2n+1)\omega$, i.e., the $1\sigma_g \rightarrow 1\sigma_u \rightarrow 2\sigma_g$ transition frequency, is accompanied by odd harmonics. This is in agreement with the quasienergy spectrum, Fig. 4, which shows all transitions (emissions) occur between different parity (+ and −) states.

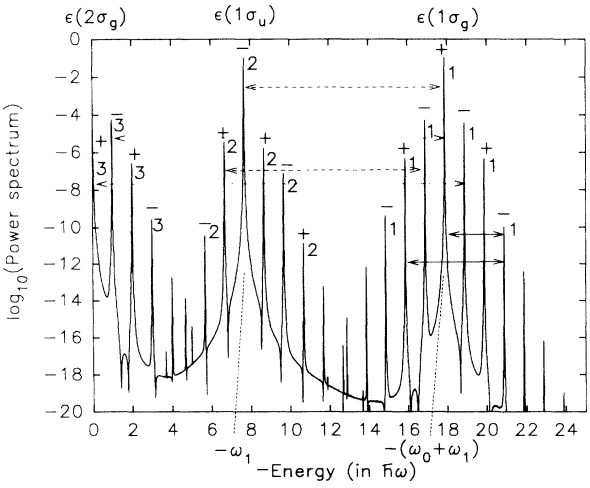

FIG. 5. Power spectrum of the time-correlation function $P(\tau)$ for Fig. 4. [$\omega_0 = \epsilon(1\sigma_u) - \epsilon(1\sigma_g) = 10.18\omega$; $\omega_1 = \epsilon(2\sigma_g) - \epsilon(1\sigma_u) = 7.67\omega$.]

III. THE NEAR-RESONANCE REGION

At the internuclear separation $R = 5$ a.u. the transition frequency between the $1\sigma_g$ and the $1\sigma_u$ state is 0.047 a.u. (about $1.1\hbar\omega$). We now enter the near-(one-photon)-resonance region. Photon-emission spectra for a two-level system resonantly driven by a relatively weak laser field have been extensively studied over the past few decades (see, e.g., the review Ref. [12]). A well-known feature of the photon-emission spectrum, Mollow's triplet [13] can be explained in a field-dressed picture as, e.g., described in Ref. [14]. Radiation emitted by a resonantly driven hydrogen atom has recently been theoretically studied by LaGattuta [15]. We will show in this work that multiple triplet structure appears for the spectrum of a resonantly driven H_2^+ molecular ion in an intense field, i.e., Mollow triplets occur at each (odd) harmonic order. We will also show that recurring triplets can be explained by a dressed picture analysis. Figure 6(a) shows the spectrum from the 3D time-dependent calculation for the H_2^+ at $R = 5$ a.u. interacting with a $\lambda = 1064$ nm, $I = 4 \times 10^{13}$ W/cm^2 laser field (with an ionization rate of 7.04×10^9/sec.). The spectrum is well reproduced by a two-level (exact) calculation as is shown by Fig. 6(b) (Rabi frequency $\Omega_R = 1.86\hbar\omega$), indicating that the resonant coupling of the $1\sigma_g$ and the $1\sigma_u$ states with the driving field dominates the whole

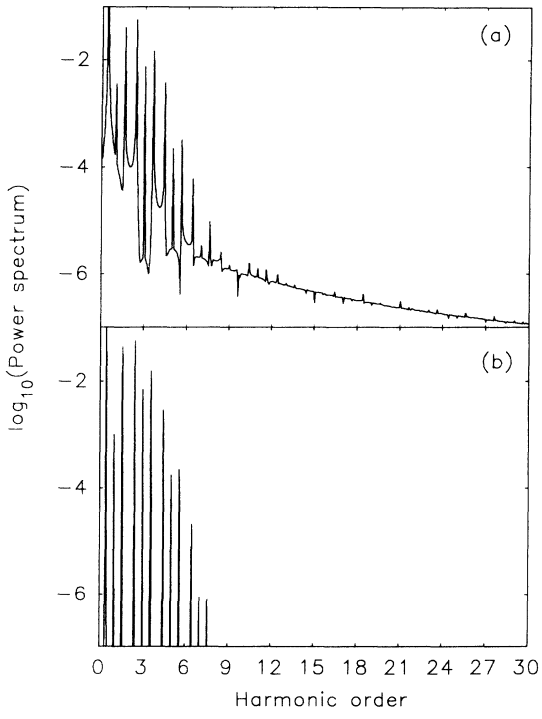

FIG. 6. Photon-emission spectrum of H_2^+ at $R = 5$ a.u., $I = 4 \times 10^{13}$W/cm^2, $\lambda = 1064$ nm. The laser pulse is given by $-E_0 f(t)\cos(\omega t)$, where $f(t) = \exp\left(-\frac{(t-t_{10})^2}{t_5^2}\right)$ for $0 < t < t_{10}$ and $f(t) = 1$ for $30 \geq t \geq t_{10}$, where $t_5 = 5$ cycles and $t_{10} = 10$ cycles. (a) 3D time-dependent exact calculation; (b) two-level calculation.

process. The strengths of these peaks quickly fall in intensity or efficiency from small to large harmonic orders, showing that the probability of the process of n-photon absorption followed by subsequently single-photon emission becomes much smaller as the number of virtually absorbed photons n increases. It is also seen that each harmonic peak (up to the seventh order) is accompanied symmetrically by two strong sidebands. The energy separations between the neighboring sidebands all take the same value. These can be explained in a dressed molecule state picture [16].

Let us denote two levels with opposite parities by $|a\rangle$ and $|b\rangle$ and define the Rabi frequency by

$$\Omega_R/2 = \langle b, n-1|V_L|a, n\rangle, \tag{15}$$

where $V_L = \mu \cdot \hat{E}$ is the two-level matter-laser interaction hamiltonian where μ is the dipole moment and $\hat{E}$ is the field operator. In the rotating-wave approximation, the dressed states are a linear superposition of the initial state a and the final state b,

$$|\pm, n\rangle = |a, n\rangle \pm |b, n-1\rangle. \tag{16}$$

Figure 7(a) shows the two-level system in the dressed representation. The $|\pm, n\rangle$ are formed due to the radiative interaction (15). The transition matrix elements for spontaneous emission between the $|\pm, n\rangle$ and the $|\pm, n-1\rangle$ states are nonzero since the spontaneous one-photon radiation matrix element

$$\langle 0_k, b, n-1|\mu \cdot \hat{E}_k|1_k, a, n-1\rangle = \langle 0_k|\hat{E}_k|1_k\rangle \mu_{ab} \neq 0, \tag{17}$$

where μ_{ab} is the transition moment and $\hat{E}_k$ is the electric field operator for the spontaneous photon of wave vector k. The $|\pm, n\rangle$ states are, therefore, radiatively coupled to the $|\pm, n-1\rangle$ states by emitting spontaneous photons at frequencies ω, $\omega \pm \Omega$. The effective frequency $\Omega = \sqrt{\delta^2 + \Omega_R^2}$ is determined by the detuning δ and the Rabi frequency Ω_R. Mollow's triplets occur as transitions at frequency Ω as illustrated in Fig. 7(a). Now let us go to higher order terms. Figure 7(b) illustrates the dressed two-level system with higher-order photon states, i.e., nonresonant states. Here the transitions induced by real resonant photon processes are marked as horizontals, those induced by virtual processes are marked by the dashed lines. The virtual transitions correspond to the fact that the matrix elements $\langle b, n+1|V_L|a, n\rangle \neq 0$. We see that, for example, the $|a, n\rangle$ state is now not only coupled to the $|b, n-1\rangle$ by the resonant photon transition but is also coupled to the $|b, n+1\rangle$ state by the virtual photon transition. Similarly, $|b, n-1\rangle$ is coupled to $|a, n-2\rangle$ state for the same reasons as above and so on. Consequently, the dressed state wave function is given by the linear superposition

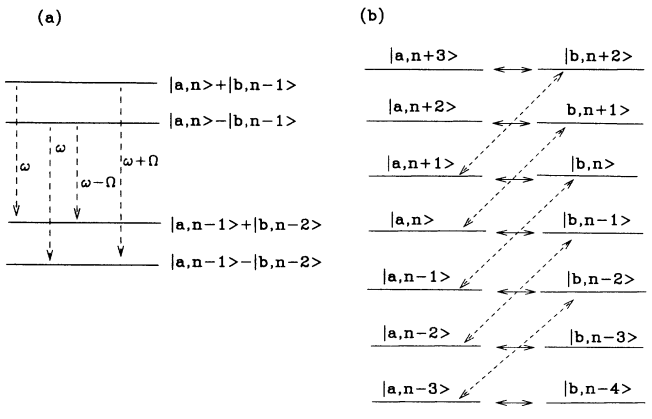

FIG. 7. The dressed energy levels of a near-resonant driven two-level system. (a) spontaneous emission for resonant states; (b) complete set of dressed states showing resonant (solid arrow line) and virtual (dashed arrow line) transitions.

$$|+, n\rangle = \alpha|a, n\rangle + \beta|b, n-1\rangle + \gamma|b, n+1\rangle + \zeta|a, n+2\rangle + \eta|a, n-2\rangle + \xi|b, n-3\rangle + \cdots, \tag{18a}$$

$$|-, n\rangle = \alpha'|a, n\rangle + \beta'|b, n-1\rangle + \gamma'|b, n+1\rangle + \zeta'|a, n+2\rangle + \eta'|a, n-2\rangle + \xi'|b, n-3\rangle + \cdots, \tag{18b}$$

where the coefficients denoted by Greek letters are, in principle, determined by the detuning and the couplings. Now it is seen, for example, that the nth dressed state contains a $|b, n-1\rangle$ component whereas the $(n-3)$th dressed state has the $|a, n-1\rangle$ component. Again due to the existence of nonvanishing spontaneous radiation matrix elements between the $|a, n-1\rangle$ and $|b, n-1\rangle$ states as in Eq. (17), the nth dressed state is therefore capable to emit photons at frequencies 3ω and $3\omega \pm \Omega'$, where Ω' is an effective Rabi frequency for that process. In a similar manner, it can be shown that the dressed state picture always predicts radiation at frequencies $(2n+1)\omega$ and $(2n+1)\omega \pm \Omega'$, i.e., multiple triplets centered on each odd harmonic. A Mollow triplet is the first order approximation to the complete picture. One way to determine the value of the effective Rabi frequency Ω' is to diagonalize the complete matrix involving all the $|\pm, n\rangle, n = 0, ..., \infty$ states illustrated in Fig. 7(b). It is worth it to note that even harmonics, i.e., the emission of $2n\hbar\omega$ energy photons is impossible from the above analysis since the n and $(n-2)$ dressed states never have a and b components with the same laser photon number [Eq. (18)], which is a prerequisite for an allowed spontaneous transtion [Eq. (17)]. It is possible, however, that the odd harmonic sidebands move to and coincide at the even harmonic $(2n\hbar\omega)$ positions for certain intensities thus giving rise to radiation of even harmonics [4,17].

An alternative way to determine the effective Rabi frequency Ω' is to numerically propagate the laser-matter system in time and calculate the time-correlation function $P(\tau)$ [Eq. (14c)]. Since the time-correlation function can be expanded by a Fourier series associated with the dressed state energies (the Floquet or quasienergies), as described by Eq. (14d), the Floquet energies (and subsequently Ω' which can be shown to have a simple relation to the difference of the Floquet energies) are then

obtained from the power spectrum of the Fourier series [Eq. (14e)]. Figure 8 shows the power spectrum of the time-correlation function for the resonantly driven two-level system. One sees pairs of identical quasienergies separated by $\hbar\omega$, one sharp and one broad and these are marked as 1 and 2. Each peak corresponds to a Floquet mode ψ_n^j [Eq. (14b)] which has a definite parity as marked with $\pm$ signs (+ for even; and − for odd) [11] (also see Sec. II). It is the transitions between these Floquet modes with the same numbers (i.e., sharp-sharp or broad-broad) and different parities that gives rise to harmonic generation, whereas those with different numbers (sharp-broad) and different parities yield the sidebands [17]. The radiation frequencies obtained from Fig. 8 match well those from Fig. 7(b), thus confirming the quasienergy contributions to the sidebands.

We emphasize that Figs. 6(a) and 6(b) correspond to the calculated *coherent* spectrum. Contributions from Raman-like processes can also occur and are therefore incoherent processes. The features of coherent scattering are evident from Fig. 6: there is much less scattering at the driving frequency and its harmonics than at the sideband frequencies. This is in agreement with two-level models [15].

IV. THE STRONG-COUPLING REGION

From molecular orbital theory, we know that the energy separation ω_0 between the H_2^+ $1\sigma_g$ and $1\sigma_u$ states decreases exponentially as the internuclear separation R increases [7]. At $R = 10$ a.u. we have that $\omega_0 = 0.014\omega$ ($\lambda = 1064$ nm) and $\Omega_R = 1.96\hbar\omega = 0.084$ a.u. (for $I = 10^{13}$ W/cm^2), i.e., we are now in a region where $\omega \gg \omega_0$ and $\Omega_R \gg \omega_0$, the strong coupling region. The strong coupling as measured by the Rabi frequency Ω_R is associated with the fact that the transition dipole moment of the charge-resonant states grows as $R/2$ asymptotically [3]. In this region, an analytic solution can be found for the two-level system interacting with a monochromatic light [14,4,18,5]. The expression of the Fourier components of the laser induced two-level dipole moment can be found, according to, e.g., Refs. [4] and [5] [by neglecting ω_0 in Eq. (A2a) of the Appendix, one can also recover similar results for the three-level case],

$$d_{2n+1} = d_{1,2}(|c_1(0)|^2 - |c_2(0)|^2)\frac{\omega_0}{(2n+1)\omega} \times J_{2n+1}(2\Omega_R/\omega)\exp[i(2n+1)\omega t], \quad (19a)$$

$$d_{2n} = d_{1,2}[c_1(0)c_2^*(0)\exp(i\Omega' t) - c_2(0)c_1^*(0) \times \exp(-i\Omega' t)]\frac{\omega_0}{2n\omega} J_{2n}(2\Omega_R/\omega)\exp(2in\omega t), \quad (19b)$$

where d_{2n+1} are the Fourier components for the odd harmonics at the frequencies $(2n+1)\omega$ and d_{2n} for the radiation at the frequencies $2n\omega \pm \Omega'$, where $\Omega' = \omega_0 J_0(2\Omega_R/\omega)$ [4].

Figure 9(a) shows the spectrum of H_2^+ at $R = 10$ a.u. for the laser condition $\lambda = 1064$ nm and $I = 10^{13}$ W/cm^2 obtained from an exact two-level time-dependent calculation. Both odd and even harmonic peaks appear although the even peaks are much weaker. The appearance of the even peaks is due to the fact that ω_0 and consequently Ω' are so small that the splitting between the $2n + \Omega'$ and $2n - \Omega'$ lines are simply indiscernible on the scale of Fig. 9(a). The strengths of the peaks are given by (19) which in turn clearly depends on the initial state of the two-level system. These initial states are completely determined by the turn on of the laser pulse

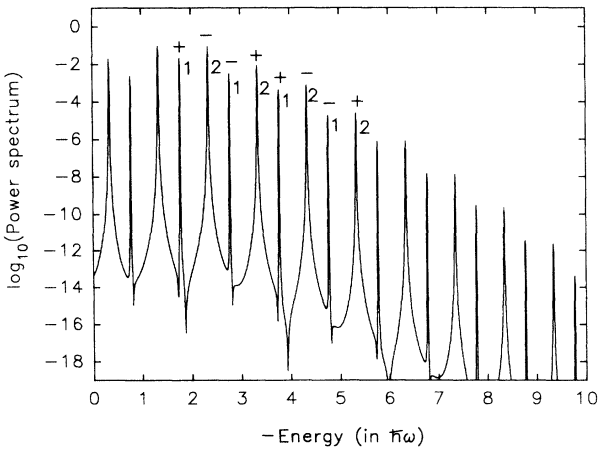

FIG. 8. Power spectrum of the time-correlation function for a two-level H_2^+ at $R = 5$, $I = 4 \times 10^{13}$ W/cm^2, $\lambda = 1064$ nm. Pairs of quasienergies ϵ_1, ϵ_2 repeat at every $\hbar\omega$.

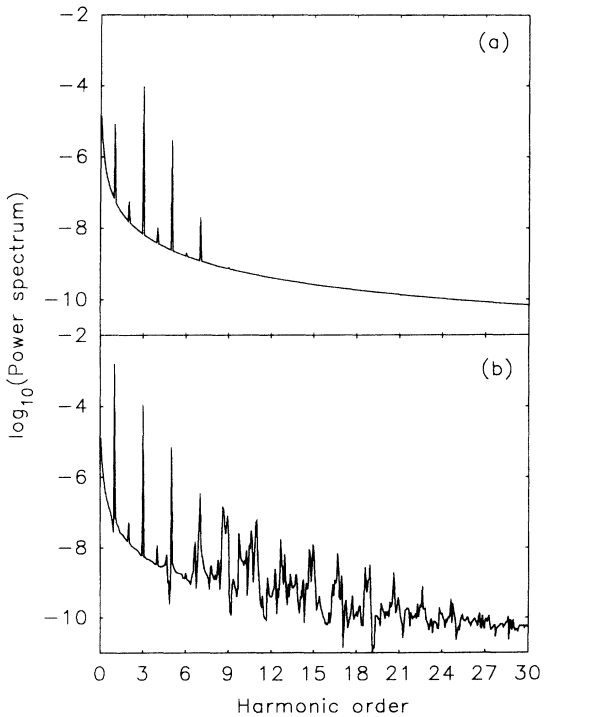

FIG. 9. Photon-emission spectrum of H_2^+ at $R = 10$ a.u., $I = 1 \times 10^{13}$ W/cm^2, $\lambda = 1064$ nm. The laser pulse shape is the same as for Fig. 6. (a) two-level calculation; (b) 3D time-dependent exact calculation.

[4,19]. Figure 9(b) shows the corresponding exact spectrum calculated by solving the total 3D time-dependent Schrödinger equation for H_2^+. Good agreement between the two calculations can be found for the third and the fifth harmonic peaks and especially, the appearance of the second, fourth, and sixth even harmonic peaks. The two spectra disagree for radiation with frequency larger than 7ω, the maximum harmonic obtained in the two-level model [Fig. 10(a)]. This must be due to radiative couplings between the $1\sigma_g$-$1\sigma_u$ CR states and upper energy surfaces (it takes about 11.3 photons to reach the closest upper level, the $3\sigma_g$). It is also seen that the strength of the first peak from the 3D calculation is two orders of magnitude larger than that from the two-level calculation. This difference reflects the coupling between the ground state and the continuum (14 photons are required for ionization) via multiphoton transitions. This coupling is ignored in the two-level calculation. With this in mind, the two-level calculation is seen to give reasonable results at $I = 10^{13}$ W/cm^2, where little ionization occurs (the ionization rate is 1.41×10^9/sec.).

Now we consider the high field case where I=10^{14} W/cm^2, $\Omega_R = 6.2\omega$. Significant ionization is observed (57% of H_2^+ is ionized by a 30 cycles laser pulse leaving to an ionization rate of 6.1×10^{12}/sec.) in this case. Figure 10(a) shows the spectrum from the two-level calculation. It again predicts both odd and even harmonics. A first plateau region is also identifiable for the spectrum with a cutoff at the eleventh harmonic order. This value of the cutoff agrees with the order $n = 2\Omega_R/\omega$, which can be obtained from the asymptotic behavior of the Bessel function $J_n(2\Omega_R/\omega)$, Eq. (19a) as discussed in detail in Ref. [5]. This corresponds to the maximum energy acquired by the electron in the two-level system in presence of the field. Figure 10(b) gives the exact spectrum from the 3D calculation. It is seen that the peaks with a cutoff up to the eleventh harmonic order (referred to as the molecular plateau [5]) appear again but are more than one order of magnitude stronger than those of the two-level model, Fig. 10(a). The even harmonics are too weak to be seen. Furthermore, a second plateau up to the 47th harmonic order which is associated with the ground-continuum coupling (referred to as the atomic plateau) can be identified. The cutoff value of the atomic plateau can be well explained by a semiclassical model of ionizing electrons [20]. We conclude that for intensities $I > 10^{14}$ W/cm^2, the two-level description is not adequate any more and coupling to continuum electronic states must be considered. This is corroborated by the exact calculations of the $1\sigma_g \rightarrow 1\sigma_u$ population difference, $|c_1(t)|^2 - |c_2(t)|^2$, which appears in the laser-induced dipole expression (19a). For an exact two-level system, this population difference should oscillate between -1 and 1 as described by Ref. [5], i.e.,

$$|c_1(t)|^2 - |c_2(t)|^2 = \cos\left(\frac{2\Omega_R}{\omega}\sin(\omega t)\right) = J_0\left(\frac{2\Omega_R}{\omega}\right) + 2\sum_{k=1}^{\infty} J_{2k}\left(\frac{2\Omega_R}{\omega}\right) \times \cos(2k\omega t). \quad (20)$$

Oscillations occur at 2ω, 4ω,..., $2k\omega$ for $\Omega_R \gg \omega$, in agreement with Fig. 11. From Fig. 11, one sees clearly these oscillations are considerably dampened due to higher level excitations and ionization. The damping rate can be estimated to be 6×10^{12}/sec., which is in agreement with the ionization rate.

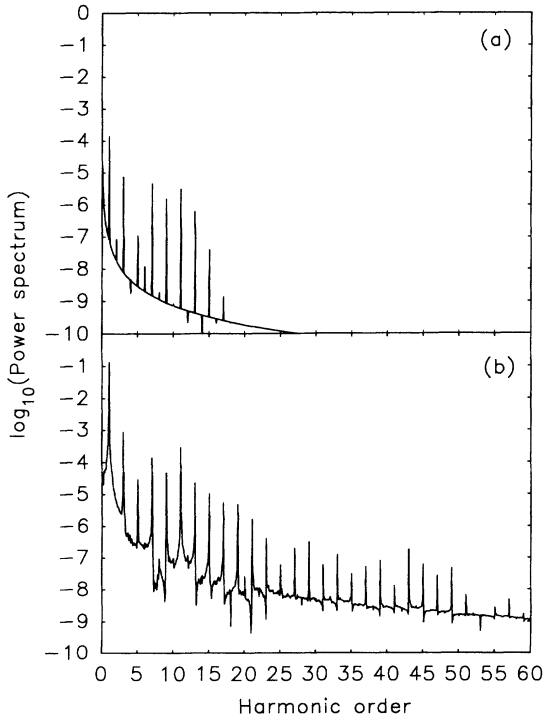

FIG. 10. Photon-emission spectrum of H_2^+ at $R = 10$ a.u., $I = 10^{14}$ W/cm^2, $\lambda = 1064$ nm. The laser pulse shape is the same as for Fig. 6. (a) two-level calculation; (b) 3D time-dependent exact calculation.

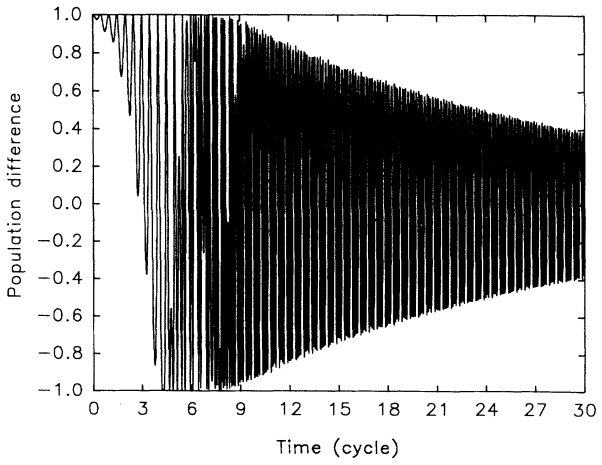

FIG. 11. Population difference $|c_1(t)|^2 - |c_2(t)|^2$, between $1\sigma_g$ and $1\sigma_u$ states in H_2^+ at $R = 10$ a.u., $I = 10^{14}$ W/cm^2, $\lambda = 1064$ nm. Oscillation frequencies follow Eq. (20). (1 cycle=3.55 fs).

V. CONCLUSIONS

In this work the photon-emission spectra of the H_2^+ molecular ion in moderately intense laser fields (10^{13} W/cm$^2 \leq I \leq 10^{14}$ W/cm^2) at $\lambda = 1064$ nm have been calculated. The dominance of the $1\sigma_g - 1\sigma_u$ charge-resonant states of the symmetric molecular ion separated by transition frequency ω_0 allows one to define three regions. The multiphoton excitation region: $\omega \ll \omega_0$; the near-resonant region: $\omega \approx \omega_0$; and the strong coupling region: $\Omega_R, \omega \gg \omega_0$, where Ω_R is the Rabi frequency, according to the variation of internuclear separation R. Simple models are compared to a rather computationally-demanding exact 3D time-dependent method. In the multiphoton excitation region, harmonic peaks, multiphoton multiplet peaks and other nonharmonic peaks coexist. It is shown that both the harmonic and the multiphoton resonance structures can be described by a two-level analytic theory based on a WKB-Mathieu equation solution. High-order nonharmonic radiation can be explained in a dressed state analysis involving more levels and frequency assignments are confirmed by calculating the Floquet (quasienergy) states from a time-correlation function. In the near-resonant region, a multiple Mollow triplet structure is obtained. This structure is explained using a dressed picture analysis for a two-level system. The splittings between the neighboring sidebands are due to transitions between field-molecule quasienergy (Floquet) states and these are confirmed by Fourier analyzing the time-correlation function of the dressed state system. The two-level description is found to be quite accurate in this resonant case. In the strong coupling region, a two-level analytic solution is shown to explain some of the key structures in the low frequency part of the photon-emission spectra, especially the splittings of the even harmonics which are shown to depend on the Bessel function $J_0(\Omega_R/\omega)$, which is a measure of the separation of the quasienergies. The two-level model is shown to become inadequate as the laser intensity increases beyond 10^{14} W/cm^2 because of its neglect of the bound-continuum or ionization transitions. A complete calculation such as the 3D time-dependent calculation employed in this work becomes necessary then. Finally, we emphasize that all calculations reported here are for single, isolated molecules. Inclusion of macroscopic effects should enhance the coherent spectrum reported here [21].

ACKNOWLEDGMENTS

The financial support from the National Centre of Excellence in Molecular and Interfacial Dynamics and the Natural Sciences and Engineering Research Council of Canada is gratefully acknowledged.

APPENDIX: THE WKB-MATHIEU SOLUTION OF AN EQUALLY SEPARATED, EQUALLY COUPLED THREE-LEVEL SYSTEM

We suppose that the total time-dependent wave function $\psi(t) = \sum_{i=1}^{3} c_i(t)\psi_i$, where ψ_i is the time-independent eigenfunctions of level i. The time-dependent Schrödinger equation for the equally separated, equally coupled three-level system interacting with a laser field is written as

$$i\dot{c_1} = -\omega_0 c_1 + \Omega_R \cos(\omega t) c_2, \tag{A1a}$$

$$i\dot{c_2} = \Omega_R \cos(\omega t)(c_1 + c_3), \tag{A1b}$$

$$i\dot{c_3} = \Omega_0 c_3 + \Omega_R \cos(\omega t) c_2. \tag{A1c}$$

Here ω is the laser frequency. The energies of levels 1, 2 and 3 have the values of $-\omega_0$, 0, and ω_0, respectively. We define the Rabi frequency $\Omega_R = d_0 E_0$, where $d_0 = d_{1,2} = d_{2,3}$ being the transition dipole moments between the first and second levels and between the second and third levels, and E_0 being the maximum absolute amplitude of the external electric field. Next we define new electronic state symmetry amplitudes $x = c_1 + c_3$ and $y = c_1 - c_3$. By adding and subtracting (A1a) and (A1c), we have

$$i\dot{x} = 2\Omega_R \cos(\omega t) c_2 - \omega_0 y, \tag{A2a}$$

$$i\dot{y} = -\omega_0 x, \tag{A2b}$$

$$i\dot{c_2} = \Omega_R \cos(\omega t) x. \tag{A2c}$$

We note first that this has the same structure as the two-level Bloch equations (see Eq. (5), Ref. [5]). Differentiating (A2a) one more time and using (A2b) and (A2c) one obtains

$$i\ddot{x} = -2\omega\Omega_R \sin(\omega t) c_2 - 2ix\Omega_R^2 \cos^2(\omega t) - i\omega_0^2 x. \tag{A3}$$

Since we will be in the regime $\omega \ll \omega_0$ (i.e., $\omega_0/\omega \approx 10$) and $\Omega_R \ll \omega_0$ (i.e., Rabi frequency less than the level separation), the term $-2\Omega_R \omega \sin(\omega t) c_2$ on the right hand side of (A3) is small compared with the other two terms and consequently neglecting this term, one obtains that

$$\ddot{x} + [\omega_0^2 + 2\Omega_R^2 \cos^2(\omega t)] x = 0, \tag{A4}$$

or

$$\ddot{x} + [\beta^2 - q\cos(2\underline{t})] x = 0. \tag{A5}$$

Here, $\beta = [(\omega_0^2 + \Omega_R^2)/\omega^2]^{1/2}$, $q = \Omega_R^2/\omega^2$, and $\underline{t} = \omega t - \pi/2$. Equation (A5) belongs to the family of the well-known Mathieu equation. Since we are in the regime where $\omega_0 \gg \Omega_R$, this implies $\beta^2 \gg q$, so that we can seek a WKB solution of the type $\exp(\pm i \int p \, d\underline{t})$ where $p = \sqrt{\beta^2 - q\cos(2\underline{t})} \approx \beta[1 - q/(2\beta^2)\cos(2\underline{t})]$ to (A5), since the exact p has no zeros or turning points. It is easy to show that the normalized WKB solution of (A5) satifies the initial conditions that when $\underline{t} = 0$, $c_1 = 1$, $c_2 = 0$, and $c_3 = 0$ is given by

$$x = \cos\left[\beta\left(\underline{t} - \frac{q}{4\beta^2}\sin(2\underline{t})\right)\right] + ib\sin\left[\beta\left(\underline{t} - \frac{q}{4\beta^2}\sin(2\underline{t})\right)\right], \tag{A6}$$

where $b = \omega_0/[\omega\beta(1 - q/2\beta^2)]$. This has the same structure as the two-level solution, Eq. (6) of Sec. II, so that the ensuing analysis in Sec. II applies. The main dif-

ference between the three-level and the two-level case, is that q is now increased by a factor of 2 in the three-level case. Thus, the argument h of the Bessel function $J_n(h)$ is also increased by a factor of 2 for calculating the harmonic and multiphoton resonant spectra [see Eqs. (11) and (13)]. This implies a stronger photon emission for the three-level case as compared to the two-level case. Of interest is that following the analysis of the Mathieu function given in Sec. II for the two-level model, the three-level model with equal energy separation and equal radiative couplings gives no resonance scattering at frequency $2\omega_0$ [22].

[1] A. L'Huillier, K. J. Schafer, and K. C. Kulander, J. Phys. B **24**, 3315 (1991).
[2] R. S. Mulliken, J. Chem. Phys. **7**, 20 (1939).
[3] A. D. Bandrauk and M. L. Sink, Chem. Phys. Lett. **57**, 569 (1978); J. Chem. Phys. **74**, 1110 (1981).
[4] M. Yu. Ivanov, P. B. Corkum, and P. Dietrich, Laser Phys. **3**, 375 (1993).
[5] T. Zuo, S. Chelkowski, and A. D. Bandrauk, Phys. Rev. A **48**, 3837 (1993).
[6] S. Chelkowski, T. Zuo, and A. D. Bandrauk, Phys. Rev. A **46**, 5342 (1992).
[7] J. C. Slater, *Quantum Theory of Molecules and Solids* (McGraw-Hill, New York, 1963), Vol. 1.
[8] *Handbook of Mathematical Functions*, edited by M. Abramowitz and I. A. Stegun (Dover, New York, 1972).
[9] J. H. Shirley, Phys. Rev. B **138**, 979 (1965).
[10] T. Millack, V. Véniard, and J. Henkel, Phys. Lett. A **176** 433 (1993).
[11] R. M. Potvliege and R. Shakeshaft, Phys. Rev. A **40**, 3061 (1989).
[12] P. L. Knight and P. W. Milonni, Phys. Rep. **66**, 22 (1980).
[13] B. R. Mollow, Phys. Rev. **188**, 1969 (1969).
[14] C. Cohen-Tannoudji, J. Dupont-Roc, and G. Grynberg, *Atom-Photon Interactions* (Wiley, New York, 1992).
[15] K. J. LaGattuta, Phys. Rev. A **48**, 666 (1993), J. Mod. Opt. **39**, 1181 (1992).
[16] E. E. Aubanel, J. M. Gauthier, and A. D. Bandrauk, Phys. Rev. A **48**, 2145 (1993).
[17] R. Bavli and H. Metiu, Phys. Rev. Lett. **69**, 1986 (1992).
[18] R. Bavli and Y. Dakhnovskii, Phys. Rev. A **48**, 886 (1993).
[19] S. Chelkowski and A. D. Bandrauk (unpublished).
[20] P. B. Corkum, Phys. Rev. Lett. **71**, 1994 (1993).
[21] J. H. Eberly and M. V. Fedorov, Phys. Rev. A **45**, 4706 (1992).
[22] T. Zuo and A. D. Bandrauk (unpublished).

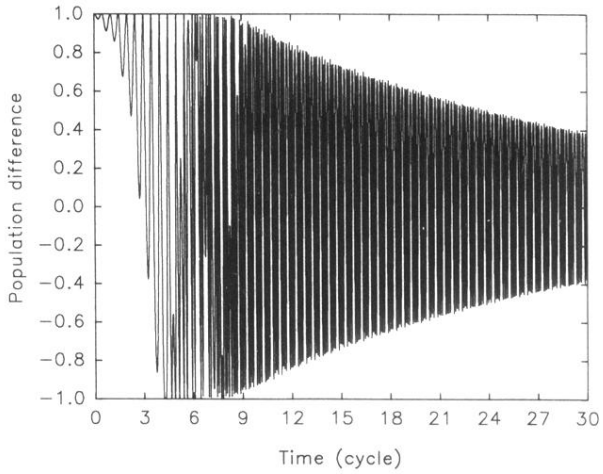

FIG. 11. Population difference $|c_1(t)|^2 - |c_2(t)|^2$, between $1\sigma_g$ and $1\sigma_u$ states in H_2^+ at $R = 10$ a.u., $I = 10^{14}$ W/cm^2, $\lambda = 1064$ nm. Oscillation frequencies follow Eq. (20). (1 cycle=3.55 fs).